Journal of Catalysis 389 (2020) 468–475

Contents lists available at ScienceDirect

Journal of Catalysis

journal homepage: www.elsevier.com/locate/jcat

Consequences of product inhibition in the quantification of kinetic parameters

James W. Harris [1], Anuj A. Verma, Jeremy W. Arvay, Arthur J. Shih, W. Nicholas Delgass *, Fabio H. Ribeiro *

Charles D. Davidson School of Chemical Engineering, Purdue University, 480 Stadium Mall Drive, West Lafayette, IN 47907, USA

ARTICLE INFO

Article history:
Received 11 April 2020
Revised 31 May 2020
Accepted 11 June 2020
Available online 20 June 2020

Keywords:
Kinetics
Oxidation
Catalysis
Inhibition

ABSTRACT

While the potential for product inhibition in catalytic reactions is well known, the impact of neglected inhibition on measured kinetic parameters is often overlooked. The presence of product inhibition, most often caused by the competitive adsorption of products with reactants on catalytic active sites, is difficult to determine *a priori* for an arbitrary catalytic system. The significance of product inhibition relies on the concentration of the products, their adsorption thermodynamics on catalytically relevant sites, and process parameters such as temperature and pressure. When inhibition is significant, however, apparent activation energies and reaction orders vary from the differential-reactor apparent activation energy by a factor of $1/(1-\delta)$, where δ is the total inhibition order (e.g., the factor $(1-\delta) = 1.6$ for a system with product inhibition of -0.6 order). This is illustrated here with the kinetics of NO oxidation over Cu ion clusters (Cu_xO_y) in Cu-SSZ-13, for which the product NO_2 inhibits the forward reaction. Furthermore, in the presence of inhibition, when only reactants are fed to a flow reactor or placed in a batch reactor, there is often no practical conversion that is low enough to guarantee differential behavior. Inclusion of products in the feed solves this problem, allowing accurate determination of kinetic parameters such as apparent reaction orders and activation energies. We also demonstrate that evaluation of the necessity of co-feeding products to assure measurement of differential-reactor data in a given catalytic system is straightforward from a plot of the log of the rate (or conversion) versus the log of the space time in a flow reactor or elapsed time in a batch reactor. We encourage inclusion of this test in all kinetic analyses that are reasonably approximated by power law rate expressions.

1. Introduction

Inhibition of the forward rate by products of the reaction is prevalent in heterogeneous catalysis. Examples include the combustion of methane on Pd [1,2], hydro-dechlorination of chlorocarbons on Pd [3,4], the water-gas shift on Pd [5], Pt [6,7], and $CuO/ZnO/Al_2O_3$ [8], SO_2 oxidation on Pt [9], NO oxidation on Cu, Fe-zeolites [10,11] and Pt [12,13], NO decomposition on Cu-zeolites [14], epoxidation of ethylene to ethylene oxide on Ag/α-Al_2O_3 [15], epoxidation of propylene to propylene oxide on Au/TS-1 [16], cyclohexene epoxidation on Ti, Ta, and Nb containing molecular sieves of the Beta topology [17], ketonization of acetic acid on both Ru/TiO_2 [18] and on H-ZSM-5 [19], and dehydrogenation of methanol to methyl formate [20]. Failure to account for product inhibition in the planning and analysis of kinetic experiments can produce significant errors in calculated kinetic parameters. The source of these errors is demonstrated in the following qualitative argument. Consider a monomolecular transformation of reactant A to product B taking place in a well-mixed, continuous stirred tank reactor (CSTR) with pure A as the sole component of the inlet stream. A typical set of experiments would vary temperature at constant concentration and flow rate of A and vary the concentration of A ($[A]$) by diluting in inert gas at constant temperature. The slope of a plot of the natural log of the rate versus inverse temperature equals the negative apparent activation energy divided by the gas constant R, and the slope of a log-log plot of rate vs. concentration of A equals the apparent reaction order of A. We will assume that even though the conversion of A is below 10% for all data gathered, the rate is inverse order in B for all measurements, and that this fact is not known to the investigator. In the activation energy experiments, as the temperature is increased the conversion will increase, increasing the concentration of B ($[B]$). At higher $[B]$ the

* Corresponding authors.
E-mail addresses: delgass@purdue.edu (W.N. Delgass), fabio@purdue.edu (F.H. Ribeiro).
[1] Current address: Department of Chemical and Biological Engineering, The University of Alabama, 3043 H. M. Comer Hall, 245 7th Avenue, Tuscaloosa, AL 35487, USA.

https://doi.org/10.1016/j.jcat.2020.06.014
0021-9517/

rate will decrease, thus diminishing the increase in rate caused by higher temperature and leading to lower apparent activation energy. This was experimentally verified by Mulla et al. [12] and Hamzehlouyan et al. [9], who studied the effect of product inhibition on the kinetics of NO oxidation and SO_2 oxidation, respectively, over supported Pt clusters and recorded a lower value of the apparent activation energy in the absence of product co-feeds. Similarly, increases in the concentration of A at constant temperature will yield more B, which will diminish the rate increase caused by A and lead to a lower than expected order in A.

Most commonly, the errors above are generated by the assumption that product inhibition of the forward rate can always be ignored when operating under conditions which maintain differential conversion of the reactants. While it is true that there will always be a conversion below which product inhibition can be ignored, we will show in the discussion below that this value of the conversion is often too low for practical experiments and that no reactor type is immune from this problem. Using NO oxidation over copper-exchanged chabazite zeolites (Cu-SSZ-13) as an example, we show that co-feeding products with the reactant mixture avoids these potential errors. We then illustrate the quantitative consequences of ignoring product inhibition. We further generalize the analysis for any power law rate expression and show that the need for co-feeding products with the reactant mixture to avoid falsification of kinetic parameter measurements can be evaluated with conversion versus space time (or, in a batch reactor, elapsed time) data. The focus of this analysis is on measurement of initial rates of reaction at conversions that are intended to be low enough to minimize effects of products on the rates. The objective of the power law rate expressions obtained from such measurements is to provide guidance, through the values of the apparent orders of reaction and the apparent activation energy and entropy, to a Langmuir Hinshelwood, Hougen-Watson rate expression representing a sequence of elementary reaction steps at the molecular level [21]. Analyses of complex reactions with kinetically important reversible steps also require data obtained with products in the feed but are beyond the scope of this paper. Detailed examples of such reactions can be found in Marin et al. [22]. We note, however, that if the reaction is irreversible and products do not undergo subsequent reactions, the analysis presented here would also apply to any incremental change in conversion with the inlet mixture representative of a specific reactant conversion. In what follows, we present a straightforward example of the issues that can arise when product inhibition is not accounted for, a simple experimental test to determine if product inhibition is occurring, and experimental strategies to accurately measure kinetic parameters in spite of inhibitory reaction products.

2. Experimental methods

2.1. Catalyst preparation

The methods for catalyst synthesis and characterization have been provided in detail elsewhere [10,23]. In brief, SSZ-13 was synthesized by following the recipe of Fickel and Lobo [24,25]. The XRD pattern, N_2 adsorption isotherms, ^{27}Al magic-angle spinning NMR, and H^+:Al ratios are reported by Bates et al. and confirm the zeolite structure and Al coordination [23]. Copper ions were deposited by a liquid phase ion exchange method by using copper nitrate as the Cu ion precursor. The catalyst used for kinetic studies reported in the main text of this manuscript had 28 ± 5% of the Cu present as Cu_xO_y species, as quantified under *in-situ* NO oxidation from separate X-ray absorption results, and the Cu:Al_{total} ratio was 0.35 as measured by AAS [10].

2.2. Catalyst characterization

Atomic absorption spectroscopy (AAS) was used to quantify bulk Si, Al, and Cu concentrations. Approximately 20 mg of sample were dissolved in 2 mL of HF (Mallenkrodt, 40 wt%) for >8 hours in a high-density-polyethylene (HDPE) bottle, then diluted with between 50 and 120 mL deionized water (Millipore, Synergy UV Water Purification System, 18.2 MΩ cm resistivity at 298 K). Proper PPE, engineering controls, and emergency exposure precautions must be taken as HF is an extremely corrosive chemical and will directly attack calcium in human tissue. 1000 ppm standards for copper (Sigma Aldrich TraceCERT, 1000 mg/L Cu in nitric acid), silicon (Sigma Aldrich TraceCERT, 1000 mg/L Si in NaOH), aluminum (Sigma Aldrich TraceCERT, 1000 mg/L Al in nitric acid), and sodium (Sigma Aldrich TraceCERT, 1000 mg/L Na in nitric acid) were diluted to two to three concentrations within the linear calibration range in clean HDPE bottles for use as standards. Elemental analysis to measure the Cu wt%, Cu:Al, and Si:Al of the dissolved sample was performed using atomic absorption spectroscopy (AAS) on a Perkin-Elmer AAnalyst 300. A calibration (absorbance vs concentration) was generated at the beginning and end of each run to ensure that absorbances did not drift by more than 5% throughout the run. Each calibration and sample bottle was shaken vigorously before collecting concentrations to eliminate possible concentration gradients due to gravimetric separation. The results of these elemental analyses are reported in Table S.1 and determined that the catalysts reported in this study had Cu weight loadings of 0–18.93 wt% Cu, Cu:Al atomic ratios of 0–1.6, and Si:Al atomic ratios of 4.3–4.5.

Powder X-ray diffraction (XRD) data were collected on a Rigaku SmartLab diffractometer using a Cu K(α) radiation source operated at 1.76 kW. Two sample holders were used. For one, approximately 0.6 g of sample were loaded in a sample holder with a depth of 2 mm. The second, about 0.05 g of sample were loaded in a sample holder with a depth of 0.2 mm. Patterns were obtained from 4 to 40° 2θ using a step size of 0.01° 2θ and scan rate 0.05° 2θ min^{-1} at ambient conditions. XRD patterns were used to confirm the presence of peaks characteristic of the CHA framework. Representative XRD patterns are reported in Fig. S.1.

Argon (87 K) adsorption isotherms were collected on a Micromeritics Accelerated Surface Area and Porosimetry (ASAP) 2020 system. Samples were first pelleted and sieved to retain particles between 180 and 250 μm in diameter, degassed by heating 0.03–0.05 g of sample to 393 K (0.167 K s^{-1}) under high vacuum (<5 μmHg) for 2 h, and then further heated to 623 K (0.167 K s^{-1}) under high vacuum (<5 μmHg) for 8 h. Extrapolation of the linear volumetric uptake during mesopore filling (~0.08–0.30 P/P_0) to zero relative pressure gave an estimate for the volume of adsorbed gas in micropores (cm^3 $(g_{cat})^{-1}$ at STP). An example Ar isotherm is reported in Fig. S.2.

UV–Visible-NIR spectra of H- and Cu-zeolites were taken at ambient conditions (calcined beforehand in air at 823 K for 6 h and exposed to air at ~298 K) with a Varian Cary 5000 UV–VIS-NIR spectrophotometer and Harrick-Scientific Praying-Mantis diffuse reflectance optics and cell. Barium sulfate ($BaSO_4$, Sigma-Aldrich, 99%) was used for zero-absorbance background scans for background correction. UV–Visible-NIR spectra were collected with a scan speed of 2000 cm^{-1} min^{-1} from 4000 to 50000 cm^{-1}. Approximately 0.1 to 0.2 g of each sample were packed and flattened in a sample cup using a clean microscope slide followed by sealing of the *in situ* cell and collection of UV–Visible-NIR spectra. For Cu-zeolites, UV–Vis-NIR spectra show two bands, which are assigned to a Cu^{2+} d-d transition at ~12000 cm^{-1} and a charge transfer (O → Cu) at ~47000 cm^{-1}, as reported in the literature [23,26,27]. Representative UV–Vis-NIR spectra are shown in Fig. S.3.

Ambient X-ray absorption spectroscopy (XAS) experiments were carried out at Sector 10 of the Advanced Photon Source at Argonne National Laboratory [28,29]. For Cu-SSZ-13 and CuO spectra using a six-shooter cell that allows the simultaneous treatment of six samples, 10–15 mg of each sample were loaded. All spectra were collected in the step scan mode. An XAS spectrum of aqueous $Cu(NO_3)_2$ was collected in a glass cuvette. For experiments using either the six-shooter cell and the glass cuvette, the Cu metal foil spectrum was calibrated to 8979 eV for the Cu K-edge. In addition, a Cu metal foil spectrum was simultaneously collected while measuring sample spectra in the energy range from 8700 eV to 9890 eV. All spectra were normalized using a first-order polynomial in the pre-edge region. XAS spectra are shown in Fig. S.4.

2.3. Catalytic testing

The reactor used for testing the kinetic effect of product co-feeding on NO oxidation was described in detail by Verma et al. [10]. In brief, kinetic experiments were performed in a plug flow reactor system which had the capability of measuring gas concentrations either from the reactor outlet or through a bypass loop. An online gas phase FTIR instrument (MKS Multigas 2030) was used with factory supplied calibrations to quantify the gas concentrations. Calibrations were validated by flowing NO and NO_2 standards (Praxair). In previous work, we have shown that catalytic dry NO oxidation (0.304 kPa NO, 0.015 kPa NO_2, 10.13 kPa O_2, 90.876 kPa N_2, 543 K) is catalyzed by Cu ion clusters (Cu_xO_y species, $x \geq 2$, $y \geq 1$), and that Cu ions electrostatically tethered to two proximal anionic framework sites in Cu-SSZ-13 are inactive for this reaction [10,30]. These results are reported in Fig. S.5, in which the NO oxidation rate is zero for samples without Cu_xO_y clusters. As a result, a candidate Cu-SSZ-13 catalyst with high Cu_xO_y content was selected for this inhibition study from a series of Cu-SSZ-13 catalysts prepared by a liquid phase ion exchange method using copper nitrate as the Cu ion precursor. Two sets of experiments were performed for this study. The first set involved quantifying the kinetics of NO oxidation in the presence of product (NO_2) co-feeding. The standard gas concentrations in this set were 0.304 kPa NO (Praxair, 3% NO in balance Ar), 0.015 kPa NO_2 (Praxair, 1.5% NO_2 in balance Ar), 10.13 kPa O_2 (Indiana Oxygen, 99.5% commercial grade), 90.876 kPa N_2 (Linde, liquid N_2 boiloff), at 543 K. The total flowrate was 1500 std cm^3 min^{-1} and the NO conversion was kept to less than 10% by varying the mass of catalyst between 30 mg and 300 mg, with most samples between 50 and 100 mg. Cu-SSZ-13 catalysts were calcined in 20% O_2 in balance N_2 at 773 K. The NO_2 inhibition was quantified by measuring the apparent reaction order with respect to NO_2, and the rate of reaction was calculated at the respective inlet concentrations on the assumption that the differential plug flow reactor could be treated as a continuous stirred tank reactor (CSTR) [31–33]. The second set of experiments involved no NO_2 co-feeding. The standard conditions were 0.304 kPa NO, 10.13 kPa O_2, 90.891 kPa N_2, at 543 K. Once again, the NO conversion was less than 10%. The inhibition effect of NO_2 was ignored and a CSTR model was used to calculate the NO oxidation rates. In both kinetic data-sets, the NO_x mass balance, defined as $(NO + NO_2)_{inlet}$ - $(NO + NO_2)_{outlet}$ was better than ±3 ppm (0.0003 kPa), which is within error of the detection limit of the FTIR instrument (MKS Multigas 2030, for which the standard deviation is ±0.5 ppm for both NO and NO_2). Lastly, all experiments were performed far away from equilibrium as quantified by $0.00\,02 < \beta \leq 0.04$, where $\beta = \frac{[NO_2]^2}{K[NO]^2[O_2]}$ is the approach to equilibrium and K is the equilibrium constant.

3. Results

3.1. Kinetic experiments in presence of NO_2 in the feed stream

When product inhibition is present, accurate kinetic parameters can only be obtained when the inhibiting product is included in the feed mixture. In order to show that NO oxidation on Cu-SSZ-13 was indeed inhibited by NO_2, the rate of NO oxidation was first evaluated on the catalyst with NO_2 co-feeding (results are designated as "dataset 1"). The NO conversion, X, was less than 10% and the overall rate of reaction was calculated using the inlet NO concentration, the space time (τ) and a CSTR model, which is valid in this instance because conversion of reactants was differential, allowing the assumption that the concentrations and reaction rate were constant across the catalyst bed. Therefore, the mass balance for a differential PFR can be simplified to that of a CSTR, and the following equations were used to calculate the rate of reaction for NO + 1/2 $O_2 \rightarrow NO_2$.

$$r_{fwd} = \frac{F_{NO_0} - F_{NO}}{N} = \frac{F_{NO_0}X}{N} = \frac{[NO]_0 X}{\tau} \quad (1)$$

where $\tau = \frac{N}{Q}$ is space time [(mol Cu) s L^{-1}], F_{NO_0} is the inlet molar flow rate of NO [(mol NO) s^{-1}], F_{NO} is the outlet molar flow rate of NO [mol NO s^{-1}], $[NO]_0$ is the inlet concentration of NO [(mol NO) L^{-1}], N is the number of moles of Cu in the catalyst [(mol Cu)], Q is the total volumetric flow rate of gas from the reactor outlet [L s^{-1}], and r_{fwd} is the moles of NO converted per mole of Cu per second [(mol NO) $(mol\ Cu)^{-1}$ s^{-1}]. Note that Q is assumed to be independent of conversion because even though moles are not conserved in the NO oxidation reaction, the concentrations of NO_x are very small relative to those of N_2 and O_2, and, at 10% NO conversion, the total flow rate would deviate by only 0.0015%, within error of the flow measurement. The rate was calculated for the standard feed conditions at each test temperature and the corresponding Arrhenius plot is displayed in Fig. 1. The apparent activation energy is 45 ± 3 kJ mol^{-1}, in agreement with values reported previously by Verma et al. [10] and identical, within error, to the apparent activation energies measured across Cu-SSZ-13 samples with a range of Cu loadings (Fig. S.6). The rate of NO oxidation at 543 K was also investigated with varied feed compositions with NO_2 included, and the apparent reaction orders with respect to NO, NO_2, and O_2 pressure were 1.5 ± 0.1, −0.9 ± 0.1, and 1.1 ± 0.1, respectively (Fig. 2). Reaction order measurements on Cu-SSZ-13 samples of varied Cu content were similar to those in Fig. 2 and are reported in Figs. S.7–S.9.

This analysis shows that NO_2 inhibits the forward rate of NO oxidation over Cu-SSZ-13. It is important to once again emphasize that this analysis rests on the assumption that the plug flow reactor is operating at a sufficiently low conversion such that the rate across the catalyst bed is invariant and therefore can be approximated as a CSTR. Since we have assumed a power law expression for the rate,

$$r_{fwd} = k_{eff}[NO]^a[O_2]^b[NO_2]^c$$

$$= k_{eff}\left([NO]_0(1-X)\right)^a([O_2]_0 - [NO]_0X/2)^b([NO_2]_0 + [NO]_0X)^c \quad (2)$$

Thus, for X sufficiently small, i.e. differential conversion, r_{fwd} is constant as shown below.

$$r_{fwd} = k_{eff}[NO]_0^a[O_2]_0^b[NO_2]_0^c \quad (3)$$

3.2. Kinetic experiments in absence of NO_2 in the feed stream

To illustrate the effect of NO_2 co-feeding on the measured kinetic parameters, data were obtained without co-feeding NO_2

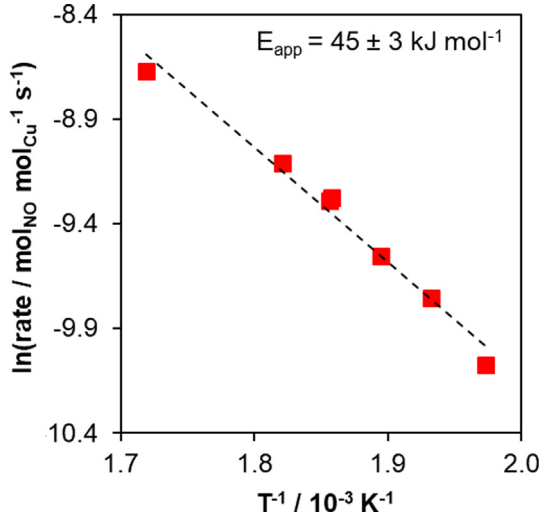

Fig. 1. Arrhenius plot for NO oxidation with NO_2 in the feed (0.304 kPa NO, 0.015 kPa NO_2, 10.13 kPa O_2, 90.876 kPa N_2, 500 to 585 K). Differential conversion in the PFR makes the measured performance equivalent to that of a CSTR. Space velocities were maintained at ~1300 s^{-1}.

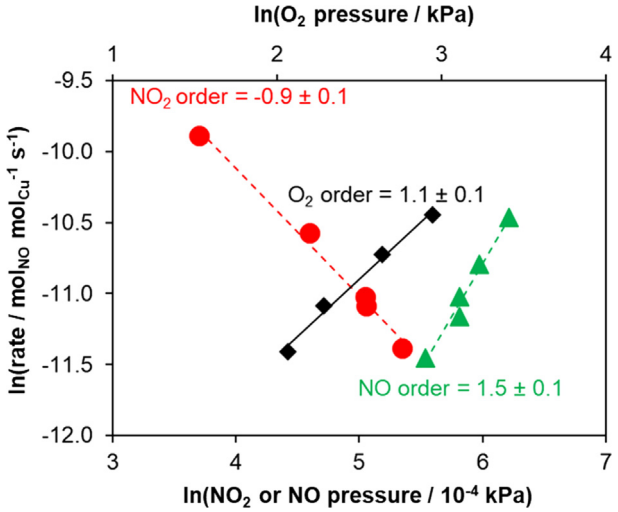

Fig. 2. Natural log of the NO oxidation rate at 543 K as a function of NO_2 pressure (●), O_2 pressure (◆), and NO pressure (▲). All kinetic data points included in this plot were obtained with NO_2 co-feeding. NO_2 pressures between 0.004 and 0.022 kPa were used for NO_2 orders. NO pressure between 0.02 and 0.05 kPa were used for NO orders, O_2 pressures between 8 and 20 kPa were used for O_2 orders. Space velocities were maintained at ~1300 s^{-1}.

for comparison to the data from Section 3.1. The NO conversion was less than 10% and the rate of NO oxidation was evaluated with the CSTR formalism described in Eq. (1), i.e. on the assumption that the reactor can be considered differential but ignoring the possible effect of NO_2 inhibition on the rate. The resulting Arrhenius plot is shown in Fig. 3. The apparent activation energy for the no NO_2 co-feeding case was 22 ± 1 kJ mol^{-1}. This value was lower than the apparent activation energy measured from NO oxidation experiments in the absence of NO_2 co-feeding by Metkar et al. (56 kJ mol^{-1}) [11] but similar to those reported by Akter et al. (17–35 kJ mol^{-1}, 500 ppm NO, 10% O_2, 373–523 K, 0.5–6 wt% Cu) [34] over Cu-CHA catalysts.

Fig. 4 shows that when NO_2 inhibition was ignored and Eq. (1) was assumed to be valid, the apparent reaction orders with respect to NO and O_2 at 543 K are 0.8 ± 0.1 and 0.5 ± 0.1 respectively. These numbers, however, differ markedly from similar kinetic estima-

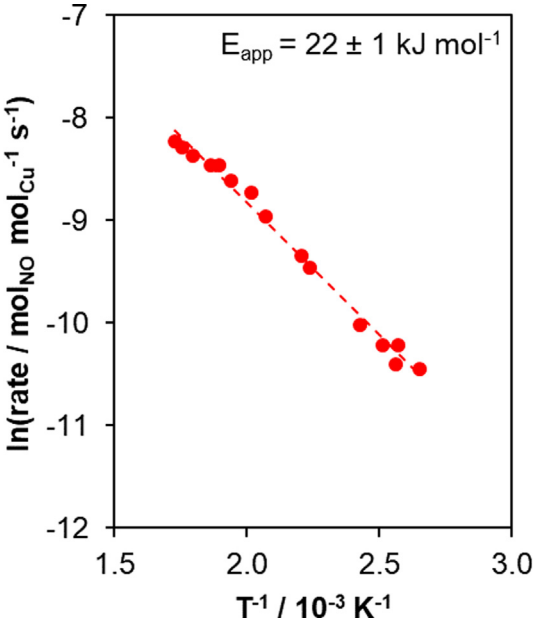

Fig. 3. Variation of the rate of NO oxidation per mole Cu with temperature, in the absence of NO_2 co-feeding, evaluated with a CSTR model and ignoring product inhibition. Feed conditions: 0.304 kPa NO, 10.13 kPa O_2, 90.891 kPa N_2, at 380–580 K. Space velocities were maintained at ~1300 s^{-1}.

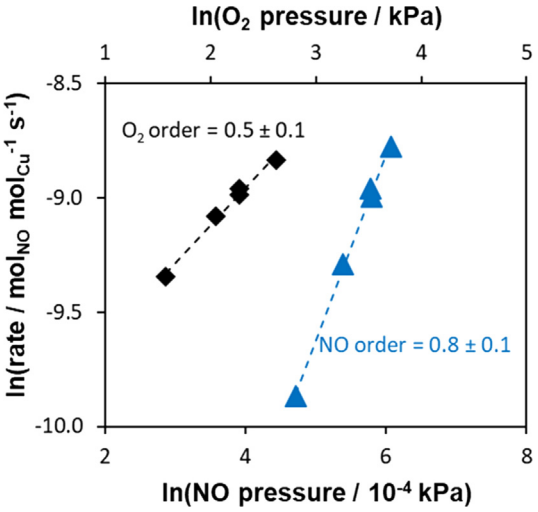

Fig. 4. Variation of the ln of the rate of NO oxidation per mole Cu, with the ln of the NO and O_2 concentrations during dry NO oxidation conditions (0.304 kPa NO, 10.13 kPa O_2, 90.891 kPa N_2, 543 K). O_2 concentrations were varied between 80 and 270 kPa while holding NO and NO_2 gas pressures constant. NO concentrations were varied between 0.024 and 0.05 kPa while holding O_2 and NO_2 gas pressure constant. NO_2 was not co-fed in the feed stream.

tions performed with NO_2 co-feeding in the feed stream (set 1). The ratio of kinetic parameters obtained from NO_2 co-feeding versus no co-feeding ($n_{cofeed} : n_{nocofeed}$) for apparent activation energy, NO order, and O_2 order are 2 ± 0.2, 1.9 ± 0.2, and 2.2 ± 0.2 respectively. This systematic trend is addressed below. We note that studies of NO oxidation on Cu-SSZ-13 at 563 K gave NO, O_2, and NO_2 orders of 0.85 to 1.0, 0.47 to 0.51, and −0.89 to −1.0, respectively [11]. In contrast to our findings at 543 K, the NO and O_2 orders did not change much in the absence of NO_2 in the feed in that study [11]. The lack of effect of the product in the feed and the relatively high value of the of the activation energy, 56 kJ mol^{-1}, measured in the 563 K range suggest that the higher temperature

can contribute to making the rate insensitive to product inhibition in the 12% conversion range, but the inhibition was clearly present at the high concentrations of NO_2 used in the apparent reaction order study [11]. A reaction order for NO of approximately unity has also been reported for NO oxidation over Cu-chabazite in the 573–673 K range in the absence of NO_2 in the feed [35]. These two studies suggest that the NO reaction order is a function of temperature and that NO_2 inhibition is significantly decreased at higher temperature but it cannot be ruled out that the detailed structure of the Cu sites in not identical to that presented here.

4. Discussion

4.1. Quantitative analysis of the NO_2 inhibition effect

The analysis of the data for NO oxidation in the absence of product NO_2 in the feed in Section 3.2 above starts with the assumption that the PFR can be presumed to be differential and therefore approximated as a CSTR. To examine this assumption more closely, we start with the general design equation for a PFR, Eq. (4).

$$\tau = [NO]_0 \int_0^X \frac{dX}{r_{fwd}} \tag{4}$$

This equation reduces to the CSTR equation (Eq. (1)) only if r_{fwd} is constant over the range of X. If we start with the power law rate expression in Eq. (2) and note that in this case $[NO_2]_0 = 0$, then at small X the rate expression becomes:

$$r_{fwd} = k_{eff}[NO]_0^{a+c}[O_2]_0^b[X]^c \tag{5}$$

Eq. (5) illustrates the source of the error that originates from neglect of product inhibition, which is specifically that the rate is a function of X and therefore of position in the plug flow reactor. Thus, integration of Eq. (4) is necessary and leads to:

$$\tau = k_{eff}^{-1}[NO]_0^{1-a-c}[O_2]_0^{-b}\int_0^X \frac{dX}{X^c} = k_{eff}^{-1}[NO]_0^{1-a-c}[O_2]_0^{-b}\left(\frac{X^{1-c}}{1-c}\right) \tag{6}$$

Solving Eq. (6) for X then leads to:

$$X = \tau^{1/(1-c)}(1-c)^{1/(1-c)}k_{eff}^{1/(1-c)}[NO]_0^{-1+a/(1-c)}[O_2]_0^{b/(1-c)} \tag{7}$$

As is true in general for plug flow reactors, since the rate changes with conversion (Eq. (5)) and conversion changes down the length of the reactor, the rate of reaction, r_{fwd}, is not directly defined by any measured parameters of the PFR experiment. If, however, we were to mistakenly assume that the reactor is differential and described by the CSTR approximation, then the forward rate of reaction would be given as $\frac{[NO]_0X}{\tau}$. Then both the order plot, Fig. 4, and the Arrhenius plot, Fig. 3, have $\ln[\frac{[NO]_0X}{\tau}]$ as the ordinate. The true expression for X, however, is given by Eq. (7) and the expression for $\frac{[NO]_0X}{\tau}$ is given by Eq. (8).

$$\frac{[NO]_0X}{\tau} = \tau^{c/(1-c)}A^{1/(1-c)}e^{-E_{app}/(RT(1-c))}[NO]_0^{a/(1-c)}[O_2]_0^{b/(1-c)}(1-c)^{1/(1-c)} \tag{8}$$

We see from Eq. (8) that the NO and O_2 orders produced from Fig. 4 are actually a/(1-c) and b/(1-c), respectively. Similarly, the Arrhenius plot of the log of $\frac{[NO]_0X}{\tau}$ versus 1/T when $[NO]_0$ and $[O_2]_0$ are held constant, Fig. 3, yields an apparent activation energy of $E_{app}/(1-c)$ from Eq. (8). Furthermore, the ratio of the true values of the orders and apparent activation energy to those measured in the absence of the inhibition product NO_2 will in each case be 1-c. Recalling that c has been found to have the value −0.9 ± 0.1, yields a value of $n_{cofeed} : n_{nocofeed}$ = 1.9 ± 0.1, in agreement with the measured kinetic ratios presented at the end of Section 3.2 above.

Finally, we show in Section S.7 that if we relax the approximation that the PFR is differential and numerically integrate the PFR equations using Eq. (2) for the rate with the values of *a*, *b*, and *c* extracted from the NO_2 co-feeding analysis above, the data give activation energy values in the agreement with those from the co-feeding experiment. This is the expected result because, as discussed, the CSTR approximation for the PFR is valid when NO_2 is co-fed.

Two important observations arise from this NO oxidation example. First, when product inhibition is present, but is overlooked, and data are obtained without the inhibiting product in the feed, serious errors are incurred in all measured kinetic parameters. This problem can be avoided by including the products in the feed at concentrations high enough that the product concentrations are also differential axially within the bed. The expected prevalence of product inhibition, generalization of the analysis, and a simple experimental test for the presence of inhibition are discussed in turn below.

4.2. Product inhibition is more likely than expected

To evaluate the likelihood of encountering product inhibition, we must first examine its origin. We begin with the simplest case. A Langmuir Hinshelwood Hougen Watson (LHHW) analysis of $A \rightarrow B$ on a catalytic surface yields:

$$r_B = \frac{kK_AP_A}{1 + K_AP_A + K_BP_B} \tag{9}$$

where *k* is the rate constant for the rate-determining step of A to B on the surface and K_A and K_B are adsorption equilibrium constants for A and B. For simplicity, assume that K_AP_A is very much less than 1. If K_BP_B is large with respect to 1, the rate will be first inverse order in B and will be decreased by the presence of B unless P_B is small enough to make $K_BP_B \ll 1$. Since $P_B = P_{A0}X_A$, where X_A is the conversion of A, there is a value of X_A below which the rate is independent of B, and that value depends on the value of K_B. Thus, it is true, as many assume, that there will always be a conversion low enough to remove the inhibition effect and guarantee differential conversion in a PFR. The question is, how low does X_A have to be? To estimate a typical value of K_B in units of atm^{-1}, we take the correlation suggested by Vannice et al. [36] for the upper bound of $-\Delta S^o_{ads}$ as 51.0–0.0014 ΔH^o_{ads}, where the entropy units are J (mol K)$^{-1}$ and the enthalpy units are J mol^{-1}. For a typical value of ΔH^o_{ads} of 84 kJ mol^{-1} (20 kcal mol^{-1}), the upper bound for $-\Delta S^o_{ads}$ would be 168 J (mol K)$^{-1}$. The lower bound reported by Vannice et al. was 41.8 J mol^{-1} K^{-1}[36]. If we approximate ΔS^o_{ads} as 105 J (mol K)$^{-1}$ (the average of 41.8 and 168 J mol^{-1} K^{-1}) and assume that the onset of inhibition will occur when K_BP_B = 0.1 (i.e., when the term for coverage of B in the denominator of a Langmuir-Hinshelwood rate expression approaches the order of magnitude of unity), Eq. (10) shows the relation between P_B (with units of Pa), ΔH^o_B (ΔH^o_{ads} for species B, J mol^{-1}), R (ideal gas constant, units J mol^{-1} K^{-1}) and T (K) at that point:

$$P_B = 0.1 * 101325 * exp\left(\left(105 + \frac{\Delta H^o_B}{T}\right)R^{-1}\right) \tag{10}$$

At 600 K, the rate of reaction of 1 atm of A (to form B) would be suppressed by competitive adsorption from B (i.e., product inhibited) at a conversion of 0.15%. This value for a reaction at atmospheric pressure shows that the standard assumption that product inhibition does not impact measured kinetic parameters at 10% conversion is not reliable and suggests that one should assume that inhibition will corrupt the observed kinetics until experiments prove otherwise. Further evaluation of the effects of parameter choice are included in the Supporting Information, Fig

S.12, and those results further support the conclusion that is it not safe to assume that an arbitrary low conversion is adequate to guarantee that inhibition can be ignored.

For our example of NO oxidation on Cu-zeolites, however, the situation is more complex, because the partial pressures of the limiting reagent are low and the reaction mechanism must be considered more carefully to include the possibility of product inhibition. We can first attempt to apply the same approach represented by Eq. (10) for the simplest general LHHW reaction A → B, however, as we see below this approach fails as the mechanism for NO oxidation is not as simple as this example reaction. Metkar et al. [11] estimated that the adsorption enthalpy for NO_2 on Cu-CHA was 141.5 kJ mol^{-1} by regressing parameters in a kinetic model. The upper bound of $-\Delta S^o_{ads}$ calculated from the Vannice correlation [36] using $\Delta H^o_{ads,NO_2}$ = −141.5 kJ mol^{-1} would be 249 J (mol K)$^{-1}$. Given the similarity between this value and the tabulated value of $-\Delta S^0$ from NIST of 269 J (mol K)$^{-1}$ [35], this approximation is not non-physical, though it would equate to near-complete entropy loss upon adsorption. Assuming the onset of inhibition occurs when the product of the adsorption constant for NO_2 and the NO_2 pressure, $K_{NO_2}P_{NO_2}$, is equal to 0.1 leads to Eq. (11) if we use the upper bound value for $-\Delta S^o_{ads}$ of 249 J (mol K)$^{-1}$,

$$P_{NO_2} = 0.1 * 101325 * exp\left(\left(249 + \frac{\Delta H^o_{ads,NO_2}}{T}\right)R^{-1}\right) \quad (11)$$

At 543 K with an NO partial pressure of 32 Pa, Eq. (11) predicts no inhibition even when the conversion approaches 100%. Inhibition is clearly present at conversions below 10%, however (Fig. 2). To see why the simple analysis behind Eq. (11) breaks down in this case, we need to look more closely at the mechanism for NO oxidation. As reported previously by Verma et al. [10], and as is compared to the series of elementary steps reported by Metkar et al. [11] in Section S.10 of the Supporting Information, a sequence of elementary steps consistent with the data is given in Scheme 1.

Assuming that the first, third, and fourth steps in Scheme 1 are in quasi-equilibrium and that *, O*, and NO_2* are the most abundant surface intermediates leads to the following rate expression:

$$r = \frac{k_2 K_1 L[O_2]}{\frac{1}{[NO]} + \frac{K_3^{-1}K_4^{-1}[NO_2]}{[NO]^2} + \frac{K_4^{-1}[NO_2]}{[NO]}} \quad (12)$$

where L is the total number of active sites, k_2 is the rate constant for step 2, and K_1, K_3, and K_4 are equilibrium constants. This expression does not have the simple LHHW form discussed above, and therefore Eq. (11) does not apply since both Eqs. (10) and (11) are derived for cases in which the inhibiting term in the denominator of the rate law follows the K_BP_B format. We see that the inhibiting terms in the denominator of Eq. (12) are ratios of equilibrium constants and the ratio of NO_2 and NO concentrations, and that product inhibition will be significant when $[NO_2]/K_4[NO]$ is large. Specifically, product inhibition will be apparent when the following equation is satisfied:

$$0.1 * \left(\frac{1}{[NO]}\right) = \frac{K_3^{-1}K_4^{-1}[NO_2]}{[NO]^2} + \frac{K_4^{-1}[NO_2]}{[NO]} \quad (13)$$

Multiplying Eq. (13) by [NO] leads to:

$$0.1 = \frac{K_3^{-1}K_4^{-1}[NO_2]}{[NO]} + K_4^{-1}[NO_2] \quad (14)$$

While it is still possible to apply an equation of the same general form as Eqs. (10) and (11) for this more complex case of equilibrium-controlled inhibition, as shown in Eq. (14), we need to know how K_3 and K_4 depend on temperature. Metkar et al. [11] provide estimates for the value of K_3 and K_4, though we note

1. $O_{2(g)} + * \leftrightarrow O_2*$
2. $NO_{(g)} + O_2* \rightarrow O* + NO_{2(g)}$
3. $NO_{(g)} + O* \leftrightarrow NO_2*$
4. $NO_2* \leftrightarrow * + NO_{2(g)}$

Scheme 1. Series of elementary steps consistent with the data collected in this manuscript and the data reported previously by Verma et al. [10].

that Verma et al. [10] wrote step four in the opposite direction versus than of Metkar et al., such that K_4^{-1} in Verma et al. [10] is equivalent to the values of K_4 reported by Metkar et al. The value $K_3^{-1}K_4^{-1}$ was estimated as 12.7exp(5200/RT) (see derivation in Section S.10), therefore the value of the second term in the denominator of Eq. (12) is equivalent to 40.2($[NO_2]/[NO]^2$) at 543 K. The value of K_4^{-1} is calculated as 1.27 * 10^{-8}*exp(141500/RT) and the right hand side of Eq. (14) equal to 0.1 when the conversion of NO to NO_2 is 0.05% (assuming an inlet NO pressure of 32 Pa and a total pressure of 101,325 Pa). Thus, inhibition would be expected when conversion is equal to or greater than 0.05%. This analysis also shows clearly that increasing temperature will decrease the coverage of O* and NO_2* and, thus, decrease the inhibition effect. Another interesting case of quasi-equilibrium control of an active intermediate by products is given was reported by Huang et al. [20]. This case shows that when the rate expression is not yet determined from data, prediction of the presence or absence of product inhibition can be difficult, and it emphasizes the need for direct experimental verification of the effect of products on the rate.

These examples serve to illustrate that the limit on conversion below which the influence of the products on the rate can be ignored can be substantially lower than is usually invoked in the literature (which is usually set at 10% conversion of reactant). Finally, we note that though we have used the simple A → B reaction as an example, any sequence of steps that involves multiple products competing for sites will generate a LHHW rate equation that will have $K_j P_j$ terms in the denominator for each product, j, and that any time a $K_j P_j$ term is order 1 or higher it has the potential to affect the rate and will do so unless a reactant term K_iP_i for adsorption of reactant i is substantially greater than K_jP_j. As also shown above, more complex sequences of steps can lead to more complex relations that determine the influence of the products on the rate.

4.3. Generalization of the analysis

First we consider a general reaction of two reactants going to two products, A + B → C + D. From the discussion above, one cannot assume, *a priori*, that the forward rate will be independent of the product concentrations, so we express the generalized power law rate as

$$r_{fwd} = k_{app} C_A^a C_B^b C_C^c C_D^d \quad (15)$$

A comparison of this rate expression to that shown in Eq. (2), shows just one additional term, involving C_D. Following the same logic as used for Eq. (2), but adding C_{Do} as well as C_{Co} to the feed to ensure differential PFR behavior, and comparing that case to the case where the effects of products are ignored leads to $n_{cofeed} : n_{nocofeed}$ = 1-c-d. This result shows that all products that affect the forward rate but are not included in the feed in kinetic experiments will lead to substantial error in the values of all measured kinetic parameters.

The analysis has so far been applied to a plug flow reactor run at low, presumed differential, conversion. The analysis of a low conversion batch reactor is identical to that shown here with τ replaced by the elapsed reaction time, t. For an ideal CSTR, where the reaction medium is well-mixed, the rate is identical at all spatial positions in the reactor and the concentrations of reactants and products are each equal to those in the reactor effluent. Under these conditions, Eq. (3) is not an approximation, but is the true representation of the rate for all conversions. For the power law rate in Eq. (15),

$$r_{fwd} = C_{Ao}X/\tau = k_{app}C_A^aC_B^bC_C^cC_D^d, \quad (16)$$

where X is the conversion of A and the concentration values of the reactants and products are those measured at the reactor effluent. If products are included in the feed and the conversion is kept sufficiently low to allow $C_i = C_{io}(1\text{-}X) = C_{io}$ for reactants and $C_j = C_{jo} + C_{Ao}\text{-}X = C_{jo}$, then,

$$r_{fwd} = C_{Ao}X/\tau = k_{app}C_{Ao}^aC_{Bo}^bC_{Co}^cC_{Do}^d, \quad (17)$$

and conversions measured at constant τ with each of the reactant and product feed concentrations varied independently will produce the data for construction of the log/log reaction order plots to produce the true reaction orders, a, b, c, and d, analogously to the procedure for the truly differential PFR in Section 3.1. If the products are not fed, however, Eq. (17) becomes,

$$r_{fwd} = C_{Ao}X/\tau = k_{app}C_{Ao}^aC_{Bo}^bC_{Ao}^cC_{Ao}^dX^{c+d}. \quad (18)$$

The rate is still given by $r_{fwd} = C_{Ao}X/\tau$, but the rate is no longer determined by the inlet concentration alone because of the X^{c+d} term. We can solve for X, however, to give,

$$X = \tau^{1/(1-c-d)}k_{app}^{1/(1-c-d)}C_{Ao}^{(a+c+d-1)/(1-c-d)}C_{Bo}^{b/(1-c-d)}. \quad (19)$$

Substituting X into the expression for the rate gives,

$$r_{fwd} = \tau^{(c+d)/(1-c-d)}k_{app}^{1/(1-c-d)}C_{Ao}^{a/(1-c-d)}C_{Bo}^{b/(1-c-d)} \quad (20)$$

Thus, we see that regardless of reactor type, ignoring product inhibition and not including products in the feed produces the same error in all the measured kinetic parameters, i.e.$n_{cofeed} : n_{nocofeed}$ = 1-c-d.

4.4. A simple test for product inhibition

It is clear that ignoring product inhibition when it is in fact present produces inaccurate kinetic data. While the solution to this problem is straightforward - including the products in the feed – the solution is not without a cost in time and effort. Re-plumbing to accommodate controlled and measured feeds of the product components may be required and measuring small changes in product concentration in the outlet versus the inlet may challenge the detection scheme. These adjustments must be made if inhibition is present, but they could be avoided if it could be shown experimentally that product inhibition does not occur in the system under study. To generate such a test, we need only to consider Eq. (19). If we maintain constant inlet reactant concentrations and vary the space time (either by changing flowrate or amount of catalyst, or both) and measure conversion, while keeping X small, a plot of ln X versus ln τ will have a slope of 1/(1-c-d). If the slope is less than 1, either c, or d, or both have measurable negative values, inhibition is indicated, and products must be fed in order to measure useful kinetic data. This approach has been demonstrated in a recent study of propylene epoxidation to propylene oxide [16]. Furthermore, it is straightforward to show that this approach also applies to a low conversion PFR or batch reactor.

The above procedure still requires that the analytical system be accurate enough to measure small conversions of reactants. One way to achieve the higher precision necessary for analysis is to add an internal standard to the feed and to measure the concentrations of reactants and products before and after the reactor for each process condition. Finally, it should be noted that this analysis is only valid for single reactions which can be defined by a power law model.

There are not many examples of direct accounting for product inhibition by comparing data in the presence and absence of products in the feed in the literature, but a few are shown below in Table 1.

5. Conclusions

In view of the importance of accurate interpretation of kinetic data to the science of catalysis and the rational design of improved catalyst formulations, the prevalence of product inhibition, and the falsification of kinetic parameters caused by overlooking product inhibition, it is prudent to account for the effects of products on the rate for all kinetic measurements. Including products in the feed is a reliable way to guarantee data integrity at a modest cost in analytical and reactor complexity. Such efforts are necessary for prediction of catalyst performance at elevated conversions (and product concentrations) relevant to industrial practice based on kinetic parameters measured in lab-scale reactors in the presence of relatively low (but consequential) product concentrations. Plotting the natural logarithm of conversion versus the natural logarithm of the space time is a simple way to check for product inhibition and a straightforward way to ascertain whether product co-feeding is necessary. We encourage inclusion of this test in all kinetic analyses that are reasonably approximated by power law rate expressions.

Declaration of Competing Interest

The authors declare that they have no known competing financial interests or personal relationships that could have appeared to influence the work reported in this paper.

Table 1
Literature examples of the quantitative effects of inhibition of products.

Overall reaction stoichiometry	Catalyst	Kinetic parameter	$n_{co-feed}$	$n_{no\ co-feed}$	$\frac{n_{co-feed}}{n_{no\ co-feed}}$
$2NO + O_2 \leftrightarrow 2NO_2$	Pt/Al_2O_3 [12]; Pt/SiO_2 [37]	E_{app} (kJ mol^{-1})	82 [12]	39 [12]; 41 [37]	2.1
		NO order	1 [12]	0.5 [37]	2
		O_2 order	1 [12]	0.5 [37]	2
		NO_2 order	−1 [12]	–	–
$CH_4 + O_2 \rightarrow CO_2 + H_2O$	Pd/ZrO_2 [2]	E_{app} (kJ mol^{-1})	170	80	2.1
		H_2O order	–	−1	–

Acknowledgments

AV and AS acknowledge funding from the National Science Foundation GOALI program under award number 1258715-CBET, and the U.S. Department of Energy vehicle technology program under contract number DE-EE0003977, and by Cummins, Inc. JH and JA acknowledge funding from the U.S. Department of Energy, Office of Basic Energy Sciences, Chemical Sciences, under grant DE-FG02-03ER15408.

Appendix A. Supplementary material

Supplementary data to this article can be found online at https://doi.org/10.1016/j.jcat.2020.06.014.

References

[1] Y.-H. Chin, C. Buda, M. Neurock, E. Iglesia, Selectivity of chemisorbed oxygen in C–H bond activation and CO oxidation and kinetic consequences for CH_4–O_2 catalysis on Pt and Rh clusters, J. Catal. 283 (2011) 10–24, https://doi.org/10.1016/j.jcat.2011.06.011.

[2] F.H. Ribeiro, M. Chow, R.A. Dallabetta, Kinetics of the complete oxidation of methane over supported palladium catalysts, J. Catal. 146 (1994) 537–544, https://doi.org/10.1006/jcat.1994.1092.

[3] F.H. Ribeiro, C.A. Gerken, G. Rupprechter, G.A. Somorjai, C.S. Kellner, G.W. Coulston, L.E. Manzer, L. Abrams, Structure Insensitivity and effect of sulfur in the reaction of hydrodechlorination of 1,1-dichlorotetrafluoroethane (CF_3–$CFCl_2$) over Pd catalysts, J. Catal. 176 (1998) 352–357, https://doi.org/10.1006/jcat.1998.2059.

[4] C.D. Thompson, R.M. Rioux, N. Chen, F.H. Ribeiro, Turnover rate, reaction order, and elementary steps for the hydrodechlorination of chlorofluorocarbon compounds on palladium catalysts, J. Phys. Chem. B 104 (2000) 3067–3077, https://doi.org/10.1021/jp992888n.

[5] L. Bollmann, J.L. Ratts, A.M. Joshi, W.D. Williams, J. Pazmino, Y.V. Joshi, J.T. Miller, A.J. Kropf, W.N. Delgass, F.H. Ribeiro, Effect of Zn addition on the water–gas shift reaction over supported palladium catalysts, J. Catal. 257 (2008) 43–54, https://doi.org/10.1016/j.jcat.2008.04.005.

[6] B. Zugic, S. Zhang, D.C. Bell, F. (Feng) Tao, M. Flytzani-Stephanopoulos, Probing the low-temperature water–gas shift activity of alkali-promoted platinum catalysts stabilized on carbon supports, J. Am. Chem. Soc. 136 (2014) 3238–3245, https://doi.org/10.1021/ja4123889.

[7] A.A. Phatak, N. Koryabkina, S. Rai, J.L. Ratts, W. Ruettinger, R.J. Farrauto, G.E. Blau, W.N. Delgass, F.H. Ribeiro, Kinetics of the water–gas shift reaction on Pt catalysts supported on alumina and ceria, Catal. Today 123 (2007) 224–234, https://doi.org/10.1016/j.cattod.2007.02.031.

[8] N.A. Koryabkina, A.A. Phatak, W.F. Ruettinger, R.J. Farrauto, F.H. Ribeiro, Determination of kinetic parameters for the water–gas shift reaction on copper catalysts under realistic conditions for fuel cell applications, J. Catal. 217 (2003) 233–239, https://doi.org/10.1016/S0021-9517(03)00050-2.

[9] T. Hamzehlouyan, C. Sampara, J. Li, A. Kumar, W. Epling, Experimental and kinetic study of SO_2 oxidation on a Pt/γ-Al_2O_3 catalyst, Appl. Catal. B Environ. 152–153 (2014) 108–116, https://doi.org/10.1016/j.apcatb.2014.01.005.

[10] A.A. Verma, S.A. Bates, T. Anggara, C. Paolucci, A.A. Parekh, K. Kamasamudram, A. Yezerets, J.T. Miller, W.N. Delgass, W.F. Schneider, F.H. Ribeiro, NO oxidation: A probe reaction on Cu-SSZ-13, J. Catal. 312 (2014) 179–190, https://doi.org/10.1016/j.jcat.2014.01.017.

[11] P.S. Metkar, V. Balakotaiah, M.P. Harold, Experimental and kinetic modeling study of NO oxidation: Comparison of Fe and Cu-zeolite catalysts, Catal. Today 184 (2012) 115–128, https://doi.org/10.1016/j.cattod.2011.11.032.

[12] S.S. Mulla, N. Chen, W.N. Delgass, W.S. Epling, F.H. Ribeiro, NO_2 inhibits the catalytic reaction of NO and O_2 over Pt, Catal. Lett. 100 (2005) 267–270, https://doi.org/10.1007/s10562-004-3466-1.

[13] J.H. Pazmiño, J.T. Miller, S.S. Mulla, W. Nicholas Delgass, F.H. Ribeiro, Kinetic studies of the stability of Pt for NO oxidation: Effect of sulfur and long-term aging, J. Catal. 282 (2011) 13–24, https://doi.org/10.1016/j.jcat.2011.05.007.

[14] B. Modén, P. Da Costa, B. Fonfé, D.K. Lee, E. Iglesia, Kinetics and mechanism of steady-state catalytic NO decomposition reactions on Cu–ZSM5, J. Catal. 209 (2002) 75–86, https://doi.org/10.1006/jcat.2002.3622.

[15] C.-J. Chen, J.W. Harris, A. Bhan, Kinetics of ethylene epoxidation on a promoted Ag/α-Al_2O_3 catalyst—the effects of product and chloride co-feeds on rates and selectivity, Chem. – Eur. J. 24 (2018) 12405–12415, https://doi.org/10.1002/chem.201801356.

[16] J.W. Harris, J. Arvay, G. Mitchell, W.N. Delgass, F.H. Ribeiro, Propylene oxide inhibits propylene epoxidation over Au/TS-1, J. Catal. 365 (2018) 105–114, https://doi.org/10.1016/j.jcat.2018.06.015.

[17] D.T. Bregante, D.W. Flaherty, Periodic trends in olefin epoxidation over group IV and V framework-substituted zeolite catalysts: a kinetic and spectroscopic study, J. Am. Chem. Soc. 139 (2017) 6888–6898, https://doi.org/10.1021/jacs.7b01422.

[18] T.N. Pham, D. Shi, D.E. Resasco, Kinetics and Mechanism of ketonization of acetic acid on Ru/TiO_2 catalyst, Top. Catal. 57 (2014) 706–714, https://doi.org/10.1007/s11244-013-0227-7.

[19] A. Gumidyala, T. Sooknoi, S. Crossley, Selective ketonization of acetic acid over HZSM-5: the importance of acyl species and the influence of water, J. Catal. 340 (2016) 76–84, https://doi.org/10.1016/j.jcat.2016.04.017.

[20] X. Huang, N.W. Cant, M.S. Wainwright, L. Ma, The dehydrogenation of methanol to methyl formate: Part I: kinetic studies using copper-based catalysts, Chem. Eng. Process. Process Intensif. 44 (2005) 393–402, https://doi.org/10.1016/j.cep.2004.05.012.

[21] M. Boudart, Kinetics on ideal and real surfaces, AIChE J. 2 (1956) 62–64, https://doi.org/10.1002/aic.690020113.

[22] G.B. Marin, G.S. Yablonsky, D. Constales, Kinetics of Chemical Reactions. Decoding Complexity, second ed., Wiley-VCH, Weinheim, Germany, 2019.

[23] S.A. Bates, A.A. Verma, C. Paolucci, A.A. Parekh, T. Anggara, A. Yezerets, W.F. Schneider, J.T. Miller, W.N. Delgass, F.H. Ribeiro, Identification of the active Cu site in standard selective catalytic reduction with ammonia on Cu-SSZ-13, J. Catal. 312 (2014) 87–97, https://doi.org/10.1016/j.jcat.2014.01.004.

[24] D.W. Fickel, R.F. Lobo, Copper coordination in Cu-SSZ-13 and Cu-SSZ-16 investigated by variable-temperature XRD, J. Phys. Chem. C 114 (2010) 1633–1640, https://doi.org/10.1021/jp9105025.

[25] D.W. Fickel, E. D'Addio, J.A. Lauterbach, R.F. Lobo, The ammonia selective catalytic reduction activity of copper-exchanged small-pore zeolites, Appl. Catal. B Environ. 102 (2011) 441–448, https://doi.org/10.1016/j.apcatb.2010.12.022.

[26] S.T. Korhonen, D.W. Fickel, R.F. Lobo, B.M. Weckhuysen, A.M. Beale, Isolated Cu^{2+} ions: active sites for selective catalytic reduction of NO, Chem. Commun. 47 (2010) 800–802, https://doi.org/10.1039/C0CC04218H.

[27] M.H. Groothaert, J.A. van Bokhoven, A.A. Battiston, B.M. Weckhuysen, R.A. Schoonheydt, Bis(μ-oxo)dicopper in Cu-ZSM-5 and its role in the decomposition of NO: a combined in situ XAFS, UV–Vis–near-IR, and kinetic study, J. Am. Chem. Soc. 125 (2003) 7629–7640, https://doi.org/10.1021/ja029684w.

[28] C.U. Segre, N.E. Leyarovska, L.D. Chapman, W.M. Lavender, P.W. Plag, A.S. King, A.J. Kropf, B.A. Bunker, K.M. Kemner, P. Dutta, R.S. Duran, J. Kaduk, The MRCAT insertion device beamline at the Advanced Photon Source, AIP Conf. Proc. 521 (2000) 419–422, https://doi.org/10.1063/1.1291825.

[29] A.J. Kropf, J. Katsoudas, S. Chattopadhyay, T. Shibata, E.A. Lang, V.N. Zyryanov, B. Ravel, K. McIvor, K.M. Kemner, K.G. Scheckel, S.R. Bare, J. Terry, S.D. Kelly, B. A. Bunker, C.U. Segre, The new MRCAT (Sector 10) Bending magnet beamline at the advanced photon source, AIP Conf. Proc. 1234 (2010) 299–302, https://doi.org/10.1063/1.3463194.

[30] C. Paolucci, A.A. Parekh, I. Khurana, J.R. Di Iorio, H. Li, J.D. Albarracin Caballero, A.J. Shih, T. Anggara, W.N. Delgass, J.T. Miller, F.H. Ribeiro, R. Gounder, W.F. Schneider, Catalysis in a cage: condition-dependent speciation and dynamics of exchanged Cu cations in SSZ-13 zeolites, J. Am. Chem. Soc. 138 (2016) 6028–6048, https://doi.org/10.1021/jacs.6b02651.

[31] D.A. Hickman, J.C. Degenstein, F.H. Ribeiro, Fundamental principles of laboratory fixed bed reactor design, Curr. Opin. Chem. Eng. 13 (2016) 1–9, https://doi.org/10.1016/j.coche.2016.07.002.

[32] V. Cybulskis, A. Smeltz, Y. Zvinevich, R. Gounder, W.N. Delgass, F. Ribeiro, Learning the fundamentals of kinetics and reaction engineering with the catalytic oxidation of methane, Chem. Eng. Educ. 50 (2016) 202–210.

[33] H.A. Massaldi, J.A. Maymó, Error in handling finite conversion reactor data by the differential method, J. Catal. 14 (1969) 61–68, https://doi.org/10.1016/0021-9517(69)90356-X.

[34] N. Akter, X. Chen, J. Parise, J.A. Boscoboinik, T. Kim, Effects of copper loading on NH_3-SCR and NO oxidation over Cu impregnated CHA zeolite, Korean J. Chem. Eng. 35 (2018) 89–98, https://doi.org/10.1007/s11814-017-0268-x.

[35] J.H. Kwak, D. Tran, J. Szanyi, C.H.F. Peden, J.H. Lee, The effect of copper loading on the selective catalytic reduction of nitric oxide by ammonia over Cu-SSZ-13, Catal. Lett. 142 (2012) 295–301, https://doi.org/10.1007/s10562-012-0771-y.

[36] M.A. Vannice, S.H. Hyun, B. Kalpakci, W.C. Liauh, Entropies of adsorption in heterogeneous catalytic reactions, J. Catal. 56 (1979) 358–362, https://doi.org/10.1016/0021-9517(79)90128-3.

[37] Y. Ji, T.J. Toops, U.M. Graham, G. Jacobs, M. Crocker, A kinetic and DRIFTS study of supported Pt catalysts for NO oxidation, Catal. Lett. 110 (2006) 29–37, https://doi.org/10.1007/s10562-006-0100-4.